SSRG International Journal of Electrical and Electronics Engineering
ISSN: 2348-8379/ https://doi.org/10.14445/23488379/IJEEE-V12I5P123

Volume 12 Issue 5, 278-286, May 2025

Original Article

Analysis of Mechanical Losses in a Squirrel-Cage Induction Motor Induced by Different Types of Eccentricity

Payal Suthar[1], Ketan Badgujar[2]

[1]*Department of Electrical Engineering, Kadi Sarva Vishwavidyalaya University, Gandhinagar, Gujarat, India.*
[2]*Department of Electrical Engineering Department, Gujarat Technological University, L. D. College of Engineering, Ahmedabad, Gujarat, India.*

[1]*Corresponding Author : suthar6482_payal@yahoo.co.in*

Received: 19 March 2025 Revised: 24 April 2025 Accepted: 05 May 2025 Published: 31 May 2025

Abstract *- Rotor eccentricity in electric machines, caused by manufacturing tolerances and rotor aging, is an inherent and unavoidable phenomenon. This eccentricity disturbs the symmetrical distribution of the magnetic field, leading to an Unbalanced Magnetic Pull (UMP) and increased bearing friction losses. This study investigates the impact of static, dynamic, and mixed types of rotor eccentricities on the mechanical losses in squirrel-cage rotor induction motors under no-load conditions. The airgap flux density was first calculated using the Magnetomotive Force (MMF) permeance method, considering multiple armature reactions. The UMP caused by the eccentricity was then determined using the Maxwell stress tensor method. The analytical results for the UMP were employed to estimate the mechanical losses, which were subsequently validated through experimental measurements. The results clearly demonstrate that the presence of rotor eccentricity substantially increases the mechanical loss component in motors, directly impacting no-load losses and consequently reducing operational efficiency. The findings underscore the critical influence of rotor eccentricity in degrading motor performance through increased friction and vibration. This study provides essential guidance for optimizing induction motor design, monitoring and maintenance to enhance reliability and efficiency and mitigate losses.*

Keywords *- Unbalanced magnetic pull, Armature reaction, Eccentricity, Airgap flux density, Ansys Maxwell, Mechanical loss.*

1. Introduction

Three-phase Squirrel-Cage Induction Motors (SCIMs) are extensively used in industrial processes because of their robust construction and simplicity. However, similar to all electrical machines, they are susceptible to various faults, with rotor eccentricity being one of the most common [1, 2]. Rotor eccentricity refers to the displacement of the rotor axis from its ideal position, leading to an uneven gap between the rotor and the stator. This misalignment can occur because of manufacturing tolerances, bearing wear, or mechanical imbalances. Eccentricity can be categorized into three types: static, dynamic, and mixed. Static eccentricity occurs when the rotor is permanently displaced from its central position, resulting in a fixed uneven air gap caused by improper assembly or bearing wear. In dynamic eccentricity, the rotor's centre is not aligned with the centre of the stator, and the rotor revolves around the centre of the stator. Consequently, the location of the minimum air gap shifts in tandem with the rotation of the rotor [3, 4]. Mixed eccentricity is a condition that involves both static and dynamic eccentricities simultaneously, in which the rotor has a fixed displacement and an additional varying component [5]. Each type of eccentricity has distinct effects on motor performance; however, in this study, we focused on mechanical losses.

Mechanical losses in squirrel cage rotor induction motors primarily due to bearing friction and windage represent a substantial portion of the total no-load losses, directly compromising overall efficiency and reliability [6]. The existing literature, directly or indirectly, indicates that rotor eccentricity significantly increases the mechanical loss of components. This is primarily due to eccentricity, which introduces a harmonic component in the magnetic field along with MMF harmonics and disturbs the uniform magnetic field distribution through a motor. This non-uniform magnetic field distribution, known as the UMP, generates an unbalanced magnetic force on the rotor [7]. This force increased the torque ripple and motor vibration, indirectly exerting an additional force on the bearing and increasing mechanical losses [8, 9]. This increased bearing load, due to eccentricity, affects the bearing life and reliability and motor performance degradation [10]. Mixed eccentricity has both fixed and varying components that contribute to an increase in the UMP, torque modulation, and bearing wear. The combined effects lead to higher vibration and a more significant reduction in torque and efficiency compared with either static or dynamic eccentricity alone [11]. The investigation of additional power loss owing to static eccentricity shows that both copper loss and core loss increase as a result of additional flux density harmonics. At the same time, mechanical loss also rises due to unbalanced magnetic forces [12]. Static eccentricity results in a non-uniform temperature distribution and elevates the peak temperature within the motor, which can reduce the lifespan of the stator insulation system [13]. An analytical tool to calculate various types of loss across various operational conditions, utilizing motor design data to predict loss influenced by factors such as voltage, load and ambient temperature in induction motors [14]. Eccentricity-induced losses adversely affects the efficiency of the induction motor. For example, 40% static eccentricity can lead to an efficiency reduction of about 1.16%, while mixed eccentricity can cause ever greater declines. These efficiency losses can have significant economic repercussions, specifically in the industrial environment [15]. From a modelling perspective, the Finite Element Analysis (FEA) and the Maxwell Stress Tensor (MST) method have been employed to evaluate the magnitude of UMP and its mechanical implications under various eccentricities [15, 16]. Similarly, the winding function theory is another approach to model the effect of non-uniform air gap on torque ripple and vibration, indirectly indicating increased mechanical stress [17]. These models provide a comprehensive understanding of motor behaviour under various eccentricity conditions by coupling electrical and mechanical equations [18].

The existing literature consistently shows that rotor eccentricity, in its static, dynamic or combined forms, profoundly alters the performance of induction motors. This influence extends to their magnetic behaviour, torque generation, vibration patterns, core losses and bearing integrity. While some work has addressed the effect of static eccentricity on mechanical losses, the limited inquiry into dynamic and mixed types represents a crucial research gap. Moreover, most findings are based on simulation analyses, with minimal experimental validation to support these findings. This highlights the need for more comprehensive experimental and analytical studies that evaluate the full spectrum of eccentricity to understand better its influence on mechanical losses, reliability and long-term motor performance.

This study addresses this gap by systematically examining the influence of static, dynamic, and mixed eccentricities on mechanical losses in squirrel cage induction motor. To achieve this, the MMF permeance wave technique is enhanced to account for the effects of primary and secondary armature reactions under no-load conditions while accounting for the MMF, slot permeance, and saturation harmonics. Using the analytical results of the gap flux density, the UMP investigated each eccentricity type using the Maxwell Stress Tensor (MST) method. Mechanical losses are then evaluated based on the approach proposed [12]. To validate the analytical model, flux density through the air gap and UMP results are compared with finite element simulations performed in commercial software ANSYS (Maxwell R19). Additionally, the mechanical loss measurements are experimentally verified through no-load and loss separation tests conducted in compliance with IEEE 112 standards [19]. These integrated analytical, simulation and experimental methods offer a more complete and accurate evaluation of how rotor eccentricity contributes to mechanical losses and impacts the overall performance of induction motors.

2 Analytical Analysis

2.1. Airgap Flux Density

Three-phase squirrel-cage induction motors with rates of 5 HP, 415 V, and 50 Hz with a symmetrical and pure sine wave supply were used for the analysis. The notations used in the analytical calculations are as follows.

n = number of slots
m = number of phases
p = number of pole pair
k,q,ε = order of harmonics
k = $6N\pm1$ ($N=\pm1, \pm2, \pm3, \ldots$)
q = $g\frac{n_r}{p}\pm k$ ($g=\pm1, \pm2, \pm3, \ldots$)
ε = $2mh+1+g\frac{n_r}{p}$ ($h=\pm1, \pm2, \pm3, \ldots$)
θ = peripheral position around the air gap

The gap flux density Equation (1) is given by the interaction between the air permeance and the MMF [20]. Under the no-load operating condition, the rotor fundamental current is negligible because the slip is closer to zero; therefore, the rotor MMF comprises rotor harmonics.

$$B_{total}=\Lambda_T\times F_T(\theta,t) \tag{1}$$

Where

$F_T(\theta,t)$ = total MMF across air gap

$= \sum_k^\infty F_{smax}\cos(\omega t-kp\theta)+ \sum_q^\infty F_{rmax}\cos(s_{k2}\omega t-qp\theta)+ \sum_\varepsilon^\infty F_{s\varepsilon max}\cos(s_{k2}\omega t-\varepsilon p\theta)$

Λ_T = total permeance of the air gap

$= \Lambda_0+\Lambda_s(\theta,t)+\Lambda_r(\theta,t)+\Lambda_{sat}(\theta,t)$

Λ_0, $\Lambda_s(\theta,t)$,$\Lambda_r(\theta,t)$, and $\Lambda_{sat}(\theta,t)$are the airgap, slotted stator, and slotted rotor permeances, respectively [21]. Therefore, the total airgap magnetic field of a healthy motor combines the fundamental components and various harmonic fields, as indicated by Equation (4).

$$B_{total} = B_f(\theta,t) + \sum(B_k(\theta,t) + B_q(\theta,t) + B_\varepsilon(\theta,t)) \quad (2)$$

The permeance equations for static [22], dynamic, and mixed eccentricity [23] are expressed by Equations (3)-(5),

$$\Lambda_{se}(\theta)=\frac{1}{\sqrt{1-\varepsilon^2}} + 2\times\frac{1-\sqrt{1-\varepsilon^2}}{\varepsilon*\sqrt{1-\varepsilon^2}}\times\cos(\theta) \quad (3)$$

$$\Lambda_{de}(\theta,t)=\frac{1}{\sqrt{1-\varepsilon^2}} + 2\times\frac{1-\sqrt{1-\varepsilon^2}}{\varepsilon*\sqrt{1-\varepsilon^2}}\times\cos(\theta-\omega_r t) \quad (4)$$

$$\Lambda_{mix}(\theta)=\frac{\mu_0}{\delta_0}[1-\varepsilon_{se}\cos\theta-\varepsilon_{de}\cos(\theta-\omega_r t)] \quad (5)$$

Where
ε_{se} = degree of static eccentricity
θ = angular position referring to the stator
ε_{de} = degree of dynamic eccentricity
ω_r $=(1-s)\frac{\omega}{p}$ = rotor's angular speed

The time harmonics are not primarily responsible for the UMP because the permeance variation does not affect the time harmonics of the magnetic flux [24]. Therefore, only space harmonics were considered to determine the gap flux density distribution. The analytical calculation considered the 3rd order of space harmonics and first-order harmonics of permeance.

2.2. UMP

AUMP is the radial electromagnetic force experienced by the rotating part owing to the uneven distribution of the air gap field. The UMP was analytically determined under three eccentricities using the MST. According to the MST method, the radial and tangential MST equations are expressed by Equations (6) and (7), respectively [25].

$$\sigma_n=\frac{b_n^2(\theta)-b_t^2(\theta)}{2\mu_0} \quad (6)$$

$$\sigma_t=\frac{b_n(\theta)b_t(\theta)}{\mu_0} \quad (7)$$

The tangential MSTσ_t is much lower than the radial component under no-load and full-load conditions. Therefore, the radial component was responsible for the UMP considered in this analytical approach.

The net force on the rotor is divided into the Y and X components, as represented by Equations (8) and (9) [25].

$$UMPy = \int_0^{2\pi} \sigma\, RL \sin(\theta)\, d\theta \quad (8)$$

The X-component is expressed by

$$UMPx = \int_0^{2\pi} \sigma\, RL \cos(\theta)\, d\theta \quad (9)$$

Hence, the resultant unbalanced magnetic pull is given by Equation (10)

$$UMP=\sqrt{UMPy^2 + UMPx^2} \quad (10)$$

2.3. Mechanical Loss Due to Eccentricity

The frictional resistance between moving components results in frictional losses converted into heat. The power lost through friction dissipates as heat increases the motor temperature. The instantaneous power loss due to friction can be calculated using Equation (11) [12].

$$p_{friction}=\mu_{fric} r f_{eq} \omega_m \quad (11)$$

Where
$p_{friction}$ = frictional losses at bearing in W
μ_{fric} = frictional coefficient depends on the bearing type (deep groove ball bearing 6306-z)
= 0.001–0.0015
f_{eq} = radial load in N
$=(\vec{w} + \overrightarrow{UMP})K$
w = rotor's weight in N
UMP = UMP in N
R = inner diameter of bearing in mt
ω_m = angular speed in radians per second

3. Model Simulations by ANSYS Maxwell

A 3D model of the three-phase squirrel-cage rotor-type induction motor was constructed, which included the rotor core, stator core, squirrel cage, shaft, and winding connection based on the specifications given in Table 1. A 3D view of the individual parts and an assembled view of the squirrel-cage induction motor are shown in Figure 1.

Table 1. Motor parameters

Stator's parameters	Number (No.) of	36
	Outer radius	85 mm
	Inner radius	51.5 mm
	Winding Connection	Delta
	Parallel winding	1
	No. of conductors per	52
	Coil pitch	8
Rotor's parameters	No. of slots	28
	Air gaps	0.3 mm
	Outer radius	51.2 mm
	Inner radius	19 mm

The electrical steel with a nonlinear B-H curve and frequency-dependent core loss data was assigned to the stator and rotor cores using predefined materials from the Maxwell material library. Half the motor's geometry is utilized to reduce the simulation time and memory requirements. This technique is commonly used when the geometry exhibits symmetry. The analysis type was set to transient solver with motion, enabling simulation of rotor rotation and resulting time-varying magnetic fields. The simulation time step was configured to capture one full electrical cycle with time settings from 0 to 0.02 s with a time step of 0.0002s.

To analyze flux variation through the airgap and the UMP, a polyline curve was created through the air gap marked in Figure 2. The field calculator was used in combination with these polylines to compute and plot flux density profiles as a function of distance or time. Three types of eccentricity were incorporated into the simulation model. To generate eccentricity (static, dynamic, and mixed), the rotating parts must shift, and either the global or relative coordinate axis must be selected as the rotational axis of the motor. In static eccentricity, the motor rotates with respect to the axis of the rotor, that is, with respect to the relative coordinate axis. In dynamic eccentricity, the rotor rotates along the axis of the stator with respect to a global coordinate system. In a mixed-eccentricity rotor, the rotor rotates in a relative coordinate system between the stator and the rotor axes.

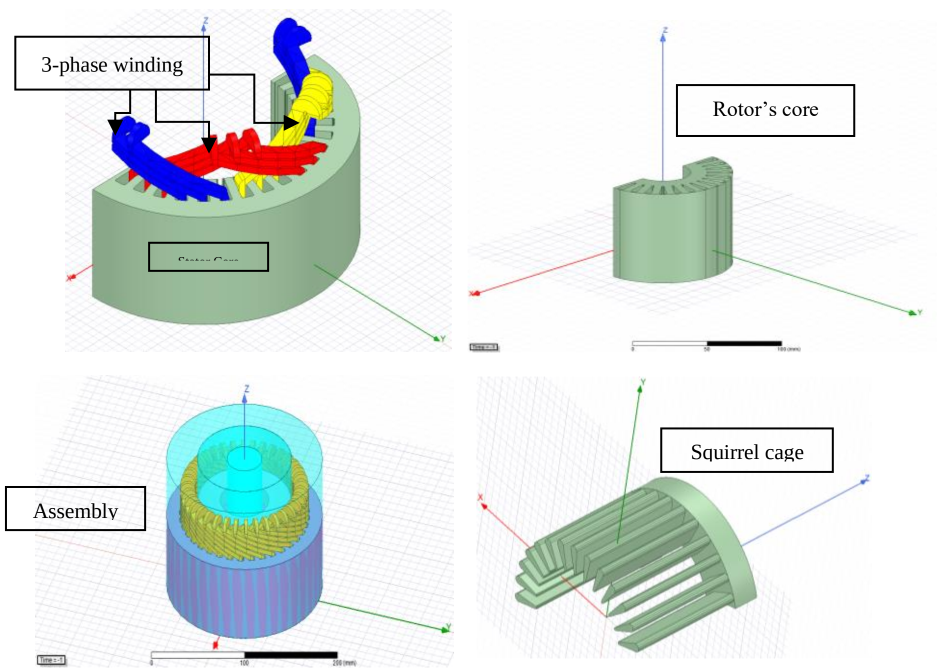

Fig. 1 Individual and assembled view of the motor

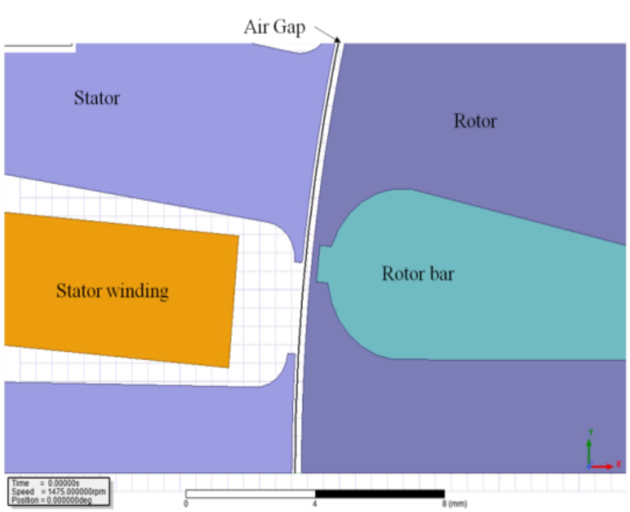

Fig. 2 Polyline through an air gap

4. Experimental Verification

To verify the analytical results of the mechanical loss, 5HP, 415 V, delta-delta-connected squirrel-cage induction motors were manufactured at JSL, Mogar, and Gujarat. The static eccentricity in the rotor was obtained via tapered machining, resulting in a minimum air gap on one side, and the position was fixed with the rotation of the rotor.

Conversely, to generate dynamic eccentricity, the rotor was machined to shift its center, causing the minimum airgap position to change with the rotor, and tapered machining of the rotor was combined with dynamic adjustment of the stator core.

The mechanical loss was calculated using the loss separation test for healthy and (12%) eccentric induction motors. These motors underwent no-load and loss separation tests in accordance with the IEEE 112 standard [19] to determine the no-load losses for a static eccentricity of 12%, dynamic eccentricity of 12%, and mixed eccentricity of 12%. Variable voltages must be applied to separate the iron, friction, and windage losses. A plot of the square value of the voltage versus the power loss needs to be constructed. The dimensions were measured using a micrometer, and the voltage, current, and input power were measured using a 0.2-class Yokogawa meter.

Figure 3 (a) and (b) show the testing and separation curves for both healthy and eccentric (static, dynamic, and mixed) induction motors.

Fig. 3 (a)Testing at JSL Industries, Ltd., Mogar
(Scale (both subplots): A distance of 1 cm corresponds to 1 foot approximately)

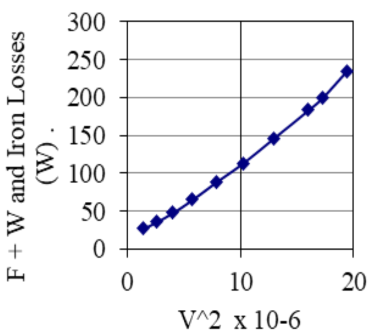

i) Separation curve for 'Healthy' induction motor

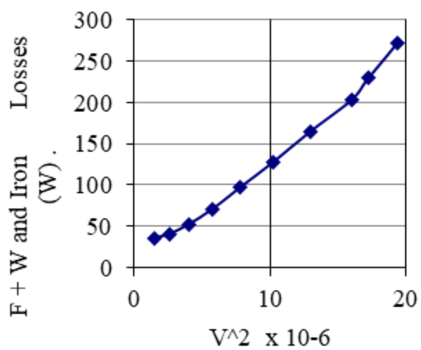

ii) Separation curve for 'Static eccentric' induction motor

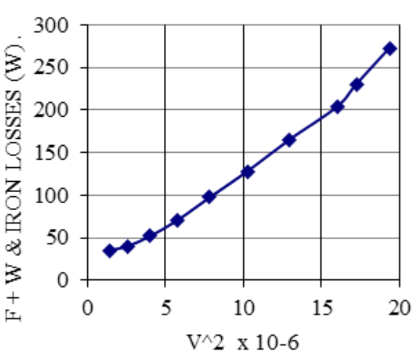

iii) Separation curve for 'Dynamic eccentric' induction motor

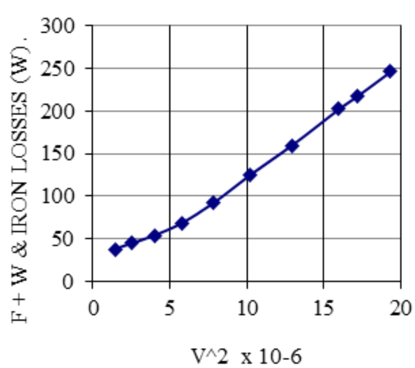

iv) Separation curve for 'Mixed eccentric' induction motor

Fig. 3(b) Separation curve for induction motor

Table 2. No-load and loss-separation test results

Operating condition	Input voltage (V)	Input current (A)	Speed (revolutions per minute)	Mechanical loss (W)
Healthy	415	3.48	1499	21
Static	415	3.6	1498	34
Dynamic	415	3.95	1497	30
Mixed	415	4.05	1495	36

5. Results and Discussion

The stator MMF is typically used to calculate the airgap flux density of a squirrel-cage induction motor under no-load conditions (Thesis, 1990b). However, under loading conditions, multiple armature reaction effects must be considered. (Wang et al., 2016) determined the gap flux density by accounting for the interaction between the stator and rotor harmonic primary armature reactions (MMFs) along with the fundamental MMF. Figure 3 compares the simulation results of the concentric rotor gap flux density distribution under no-load operating conditions with the analytical airgap flux density results, both with and without accounting for multiple armature reactions. This comparison indicates that when accounting for the armature reaction, the gap flux density value is more closely aligned with the simulation results than the value obtained without considering the armature reaction. This analytical analysis considered harmonics up to the 3rd order spatial harmonics and 1st-order slot harmonics. This technique can be further refined by incorporating higher-order harmonics. Table 3 lists the effects of the eccentricity on the maximum gap flux density. Eccentricity influences the airgap permeance, resulting in an uneven magnetic flux distribution. In the event of a static eccentricity, the concentration of the gap flux density increases at the shortest airgap distance where the rotor moves closer to the stator; hence, the peak flux density through an air gap is increased. While in dynamic eccentricity, the value of the airgap flux density varies dynamically and creates peaks during rotation, ultimately increasing the crest value of the gap flux density wave. Mixed eccentricity is associated with the co-occurrence of both effects, which ultimately increases the crest value of gap flux density.

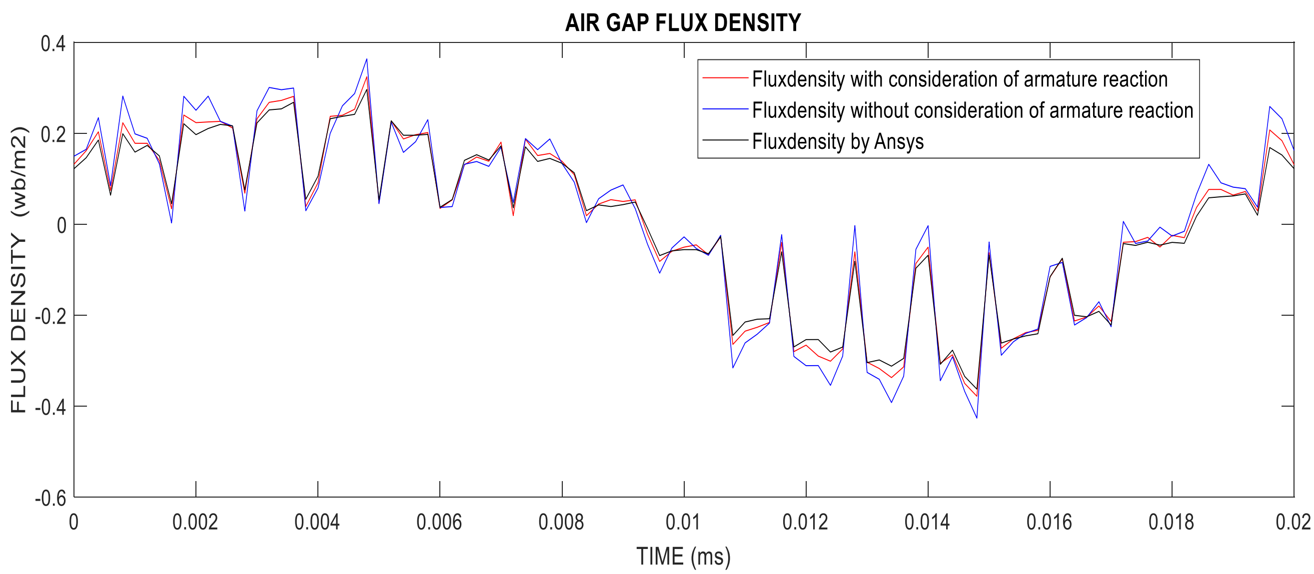

Fig. 4 Flux density plots as a function of time through the airgap under healthy operating conditions

Table 3. Maximum values of flux density through an airgap

Induction Motor Condition	Absolute maximum flux density values through an air gap (in Wb/m^2)					
	10.66%		12%		13.33%	
	Analytical	Simulation	Analytical	Simulation	Analytical	Simulation
Static	0.3589	0.3478	0.4244	0.4232	0.4221	0.4422
Dynamic	0.3590	0.3486	0.4267	0.4234	0.4210	0.4418
Mixed	0.3492	0.3493	0.4295	0.4266	0.4249	0.4478

Table 4. Absolute average values of UMP

Induction Motor Condition	Average Unbalanced Magnetic Pull (UMP) values (in kN)					
	10.66%		12%		13.33%	
	Analytical	Simulation	Analytical	Simulation	Analytical	Simulation
Static	2.90	2.83	3.97	3.92	3.98	3.94
Dynamic	2.43	2.35	3.58	3.49	3.60	3.62
Mixed	2.77	2.74	3.92	3.86	3.93	3.88

Table 5. Practical verification of mechanical loss at an eccentricity of 12%

Induction Motor Condition	Mechanical loss (in W) at an eccentricity of 12%	
	Analytical	Practical
Healthy	24	21
Static	35	34
Dynamic	32	30
Mixed	37	36

Table 4 compares the analytical and numerical results for the average value of the UMP at different levels and eccentricities. Different types of eccentricity lead to unequal magnetic forces on the rotor owing to the uneven distribution of flux density through the air gap. The UMP value depends on the direction and level of eccentricity. As the level of eccentricity increased, the UMP also increased. Static eccentricity, which remains constant with respect to the rotor position, may produce a more predictable and stable UMP. Dynamic eccentricity caused an additional harmonic in the magnetic field and magnetic forces and induced rotations at the speed of the rotor, resulting in no relative speed between the magnetic force and rotor.

Table 5 compares the practical and analytical results for the mechanical losses. (13) shows the relationship between the radial load and mechanical losses when the case in which the rotor and stator axes do not coincide; this configuration disturbs the even distribution of the magnetic force on the rotor. This uneven distribution of magnetic force results in vibration, additional friction, and wear of the motor bearings.

Therefore, the mechanical losses of the motor increase owing to the eccentricity. Dynamic eccentricity causes the rotor to oscillate, and the forces acting on the bearings fluctuate. These fluctuations increased the mechanical losses of the motor but were less severe than the effects attributed to static eccentricity. Mixed eccentricity is a mixture of static and dynamic eccentricities that exerts constant and fluctuating forces on motor bearings. In other words, eccentricity increased the motor's no-load current, as shown in Table 2. This also increased the no-load torque. As the no-load torque increased, the no-load speed decreased, and the mechanical losses of the motor increased. Despite the detailed theoretical analysis and good correlation between analytical, simulation, and experimental results, the primary limitation of the study is its focus on no-load operating conditions when investigating the impact of static, dynamic, and mixed types of rotor eccentricities on mechanical losses in squirrel-cage rotor type induction motors. Moreover, the harmonics consideration is limited to the 3rd-order spatial and 1st-order slot harmonics, potentially overlooking the influence of higher-order harmonic contributions to flux distortion and mechanical stress.

6. Conclusion

This study provides a detailed theoretical investigation of the airgap magnetic flux density by considering the effects of multiple armature reactions, even under no-load operating conditions. A strong correlation is observed between the analytical and simulation results of the gap-flux density (Figure 3) and UMP. Furthermore, comparing the experimental and analytical results for the mechanical loss yields satisfactory agreement.

In practical applications, most induction motors experience a certain level of eccentricity that increases over time. This progressively increasing eccentricity induces UMP, increases mechanical losses, and results in uneven temperature distribution. The analysis presented in this study offers a streamlined yet effective approach for evaluating these effects and provides valuable insights for assessing motor performance under eccentricity conditions.

Future research can extend this study by analyzing the impact of various types and degrees of eccentricity on the mechanical losses of induction motors under load conditions where armature reactions and electromagnetic interactions are more complex and representative of real-world scenarios.

Acknowledgments

Author 1 prepared the manuscript and Author 2 contributed with his expert review and suggestions as well as guidance for the entire manuscript.

References

[1] S. Nandi, H.A. Toliyat, and X. Li, "Condition Monitoring and Fault Diagnosis of Electrical Motors - A Review," *IEEE Transactions on Energy Conversion*, vol. 20, no. 4, pp. 719-729, 2005. [CrossRef] [Google Scholar] [Publisher Link]

[2] Alberto Bellini et al., "Advances in Diagnostic Techniques for Induction Machines," *IEEE Transactions on Industrial Electronics*, vol. 55, no. 12, pp. 4109-4126, 2008. [CrossRef] [Google Scholar] [Publisher Link]

[3] Hanifi Guldemir, "Detection of Airgap Eccentricity Using Line Current Spectrum of Induction Motors," *Electric Power Systems Research*, vol. 64, no. 2, pp. 109-117, 2003. [CrossRef] [Google Scholar] [Publisher Link]

[4] Xiaodong Li, Qing Wu, and Subhasis Nandi, "Performance Analysis of a Three-Phase Induction Machine with Inclined Static Eccentricity," *IEEE Transactions on Industry Applications*, vol. 43, no. 2, pp. 531-541, 2007. [CrossRef] [Google Scholar] [Publisher Link]

[5] Jawad Faiz, Iman Tabatabaei, and E. Sharifi-Ghazvini, "A Precise Electromagnetic Modeling and Performance Analysis of a Three-Phase Squirrel-Cage Induction Motor under Mixed Eccentricity Condition," *Electromagnetics*, vol. 24, no. 6, pp. 471-489, 2004. [CrossRef] [Google Scholar] [Publisher Link]

[6] A.K. Sawhney, and A. Chakrabarti, "*Electrical Machine Design*, DhanpatRai and Co, pp. 140-230, 2006. [Google Scholar]

[7] Andrej Burakov, *Modelling the Unbalanced Magnetic Pull in Eccentric-Rotor Electrical Machines with Parallel Windings*," Helsinki University of Technology, Espoo, Finland, pp. 1-72, 2007. [Google Scholar] [Publisher Link]

[8] Haoyu Kang et al., "Analysis of Influence of Rotor Eccentricity in Double Fed Induction Machine," *2023 6th International Conference on Power and Energy Applications*, Weihai, China, pp. 38-43, 2023. [CrossRef] [Google Scholar] [Publisher Link]

[9] Haiyang Li et al., "A Numerical Study of Rotor Eccentricity and Dynamic Load in Induction Machines for Motor Current Analysis Based Diagnostics," *Maintenance, Reliability and Condition Monitoring*, vol. 1, no. 2, pp. 71-86, 2021. [CrossRef] [Google Scholar] [Publisher Link]

[10] Jan Sobra et al., "Analysis of Rotor's Eccentricity Influence on Bearing Load of Induction Machine," *Proceedings of the 16th International Conference on Mechatronics, Mechatronika 2014*, Brno, Czech Republic, pp. 71-78, 2014. [CrossRef] [Google Scholar] [Publisher Link]

[11] Ranjan Sasti Charan Pal, and Amiya Ranjan Mohanty, "A Simplified Dynamical Model of Mixed Eccentricity Fault in a Three-Phase Induction Motor," *IEEE Transactions on Industrial Electronics*, vol. 68, no. 5, pp. 4341-4350, 2021. [CrossRef] [Google Scholar] [Publisher Link]

[12] H. Chuan, and L. Gan, "Investigation of the Power Losses in Induction Machines with Rotor Eccentricity," *Electrical Engineering*, vol. 102, no. 3, pp. 1393-1403, 2020. [CrossRef] [Google Scholar] [Publisher Link]

[13] Bruno Baptista et al., "Temperature Distribution Inside a Three-Phase Induction Motor Running with Eccentric Airgap," *Przeglad Elektrotechniczny*, vol. 88, no. 1A, pp. 96-99, 2012. [Google Scholar] [Publisher Link]

[14] Shahab Khalghani, "*Analytical Loss Calculation Tool for an Induction Motor*," Diploma Thesis, Lappeenranta-Lahti University of Technology LUT, pp. 1-50, 2020. [Google Scholar] [Publisher Link]

[15] Ogbonnaya I. Okoro et al., "Performance Comparison of Static Eccentricity Between Squirrel-Cage Induction and Wound-Field Flux Switching Machines," *International Conference on Electrical Machines*, Torino, Italy, pp. 1-6, 2024. [CrossRef] [Google Scholar] [Publisher Link]

[16] Jawad Faiz et al., "Finite-Element Transient Analysis of Induction Motors Under Mixed Eccentricity Fault," *IEEE Transactions on Magnetics*, vol. 44, no. 1, pp. 66-74, 2008. [CrossRef] [Google Scholar] [Publisher Link]

[17] Mansour Ojaghi, and Samaneh Nasiri, "Modeling Eccentric Squirrel-Cage Induction Motors with Slotting Effect and Saturable Teeth Reluctances," *IEEE Transactions on Energy Conversion*, vol. 29, no. 3, pp. 619-627, 2014. [CrossRef] [Google Scholar] [Publisher Link]

[18] Xiaowen Li et al., "Angular-Based Modeling of Unbalanced Magnetic Pull for Analyzing the Dynamical Behavior of a 3-Phase Induction Motor," *Journal of Sound and Vibration*, vol. 494, 2021. [CrossRef] [Google Scholar] [Publisher Link]

[19] "*112-2017 - IEEE Standard Test Procedure for Polyphase Induction Motors and Generators*," IEEE Standards, pp. 1-115, 2018. [CrossRef] [Publisher Link]

[20] Ali Rezig et al., "Effect of Rotor Eccentricity Faults on Noise Generation in Permanent Magnet Synchronous Motors," *Progress in Electromagnetics Research C*, vol. 15, pp. 117-132, 2010. [CrossRef] [Google Scholar] [Publisher Link]

[21] Anil Balan, "*Determination of Radial Electromagnetic Forces in Squirrel-Cage Induction Motors*," M.Sc Thesis, University of Saskatchewan, pp. 1-184, 1990. [Google Scholar]

[22] T.A. Sarikaya, A. Polat, and L.T. Ergene, "Diagnosis of Different Eccentricity Faults in Induction Motors Based on Electrical and Magnetic Signatures and Unbalanced Magnetic Pull," *Proceedings 2019 International Aegean Conference on Electrical Machines and Power Electronics, ACEMP 2019 and 2019 International Conference on Optimization of Electrical and Electronic Equipment*, Istanbul, Turkey, pp. 186-190, 2019. [CrossRef] [Google Scholar] [Publisher Link]

[23] Carlo Concari, Giovanni Franceschini, and Carla Tassoni, "Towards Practical Quantification of Induction Drives Mixed Eccentricity," *IEEE Transactions on Industry Applications*, vol. 47, no. 3, pp. 1232-1239, 2011. [CrossRef] [Google Scholar] [Publisher Link]

[24] Vladimir Kindl et al., "Review of Time and Space Harmonics in Multi-Phase Induction Machine," *Energies*, vol. 13, no. 2, pp. 1-17, 2020. [CrossRef] [Google Scholar] [Publisher Link]

[25] Mattias Wallin, "*Measurement and Modelling of Unbalanced Magnetic Pull in Hydropower Generators*," PhD Thesis, University of Uppsala, pp. 1-62, 2013. [Google Scholar] [Publisher Link]